Regimes of Arc Plasma Flow at Low Pressure

A. Kamiñska, M. Dudeck

Regimes of Arc Plasma Flow at Low Pressure

A. Kamińska ([1]) and M. Dudeck ([2,*])

([1]) Institute of Electric Power Engineering, Poznań University of Technology, 60 965 Poznań, Poland
([2]) Laboratoire d'Aérothermique du CNRS and Université de Paris 6, 92190 Meudon, France

(Received 10 May 1996, revised 8 October 1996, accepted 15 October 1996)

PACS.52.50.Dg – Plasma sources
PACS.52 75.Hn – Plasma torches
PACS 52.80 Mg – Arcs, sparks, lightning

Abstract. — The subsonic plasma jets with the diffusive shapes and supersonic cylindrical jets in argon and nitrogen in low pressure chamber using the plasma torch with segmented anode were generated. These plasma flow regimes are obtained for specified conditions of plasma torch operating parameters and pressure in chamber. Based on the LTE assumption, simple calculations have been performed for predicting the conditions of generating supersonic and subsonic plasma jets. These calculations allow to analyse the temperature, velocity and shape of plasma jets for operating parameters of plasma torch such as arc current, gas flow rate and pressure in the chamber. The energy transfer for subsonic and supersonic jets is also calculated and discussed.

Résumé. — Des jets de plasma, subsoniques avec une forme diffusive ou supersoniques et cylindriques ont été obtenus avec de l'argon et de l'azote dans une chambre à basse pression utilisant une source à plasma avec une anode segmentée. Ces régimes d'écoulement sont obtenus pour des conditions spécifiques de pression dans la chambre et de fonctionnement de la source. À partir de l'hypothèse d'équilibre thermodynamique local, un simple calcul a montré que l'on pouvait définir les conditions permettant d'obtenir des jets soit subsoniques soit supersoniques et analyser la température, la vitesse et la forme des jets de plasma pour différentes conditions de fonctionnement de la source en intensité du courant d'arc et en pression dans la chambre. Les transferts énergétiques pour des jets subsoniques et supersoniques ont été calculés et discutés.

1. Introduction

Plasma torches have become very important for many industrial applications such as plasma spraying, powder processing, welding, cutting, waste treatment, gas pollution and for aerospace researches, mainly to provide a test-environment for thermal loading of materials for the simulation of re-entry conditions by a space vehicle through upper atmospheric regions. The plasma torches using an electric arc allow to produce stationary and ionized gas at low pressure, between 10 and some thousands Pa with a temperature lower than 2 eV. A wide range of technological variations in plasma torch is available to influence the plasma properties, such as

(*) Author for correspondence (e-mail: dudeck@cnrs-bellevue.fr)

divergent or cylindrical anodes, magnetic stabilization fields, vortex, cascaded arc The plasma can be produced using arc operated for a wide range of currents (5–4000 A)

In this paper, we present different regimes of plasma flow obtained in low pressure chamber using a plasma torch with segmented and cylindrical anode. We show the possibility to obtain the subsonic plasma jets with the diffusive forms and supersonic cylindrical jets with argon or nitrogen. The different plasma jets are obtained for specified conditions of plasma torch operating parameters and pressure in chamber. In our experiments we use arc currents between 80 and 300 A with pressure of 10 to 100 kPa. For these conditions the electron density in the arc and in the core of plasma jet determined from Saha equilibrium equation is around 10^{22} m^{-3}. It is mostly agreed, that LTE should occur for electron number densities higher than 5×10^{21} m^{-3} [1,2]. Because this criterion is usually valid in the core region of a high-current arc, it has been usually considered that for high-current arcs, the plasma in the core region of the arc is generally in LTE [3–5]. Although the electron number density is higher than minimum density for which LTE exists, the departures from LTE have been observed for high speed plasma jets [6–8]. However, experimental and theoretical investigations [9–11] allow to assume that for considering conditions of temperature, velocity and pressure, the plasma is closed to LTE. Therefore, based on LTE assumption, simple calculations have been performed for predicting the conditions of generating supersonic and subsonic plasma jets. These calculations are used to analyse the temperature, velocity and shape of plasma jets for operating parameters of plasma torch such as arc current, gas flow rate and pressure in the chamber. The energy transfer for subsonic and supersonic jets is also calculated and discussed. It is shown that the energy balance is sufficient to describe the gas in the plasma source, without solving the total set of equations [10,11].

2. Description of the Plasma Torch

The experiments were carried out with a vortex stabilized plasma torch (Fig. 1). The cathode is a 8 mm long, 6 mm diameter tungsten rod, mounted on a water-cooled support. The cathode is movable in the plasma torch by the intermediary of screwed device allowing the adjustment of the distance between anode and cathode. The channel of the plasma torch is composed of water-cooled cylindrical segments made of copper, with an inner diameter of 12 mm and a length of 30 mm. The segments are insulated from each other by discs with tangential gas injection channels. The tangential gas injection produces a vortex effect in the plasma torch channel that stabilizes the plasma arc. Different gases can be injected through the insulating discs. The electric arc is initiated between the cathode and the anode or between the cathode and one of the segment, thus allowing to choose the arc length.

The plasma torch is mounted on a low pressure chamber with a length of 540 mm and an inner diameter of 115 mm

3. Analysis

3.1. Temperature and Velocity of Plasma Jet. — The different tests have led to the conclusion that the best conditions for the stationary plasma jet production are obtained with an arc of a length of some millimeters formed between the cathode and the first segment and for a jet stabilized in the chamber of the plasma torch constituted by several segments. For the description of the arc and the jet located in the chamber of the plasma torch several simplifications are assumed. The energy distribution function of all particles is isotropic. The arc and the jet are formed in the core of the vortex where the pressure is constant and the column of arc and the jet is cylindrical. In this zone, the flow can be considered as

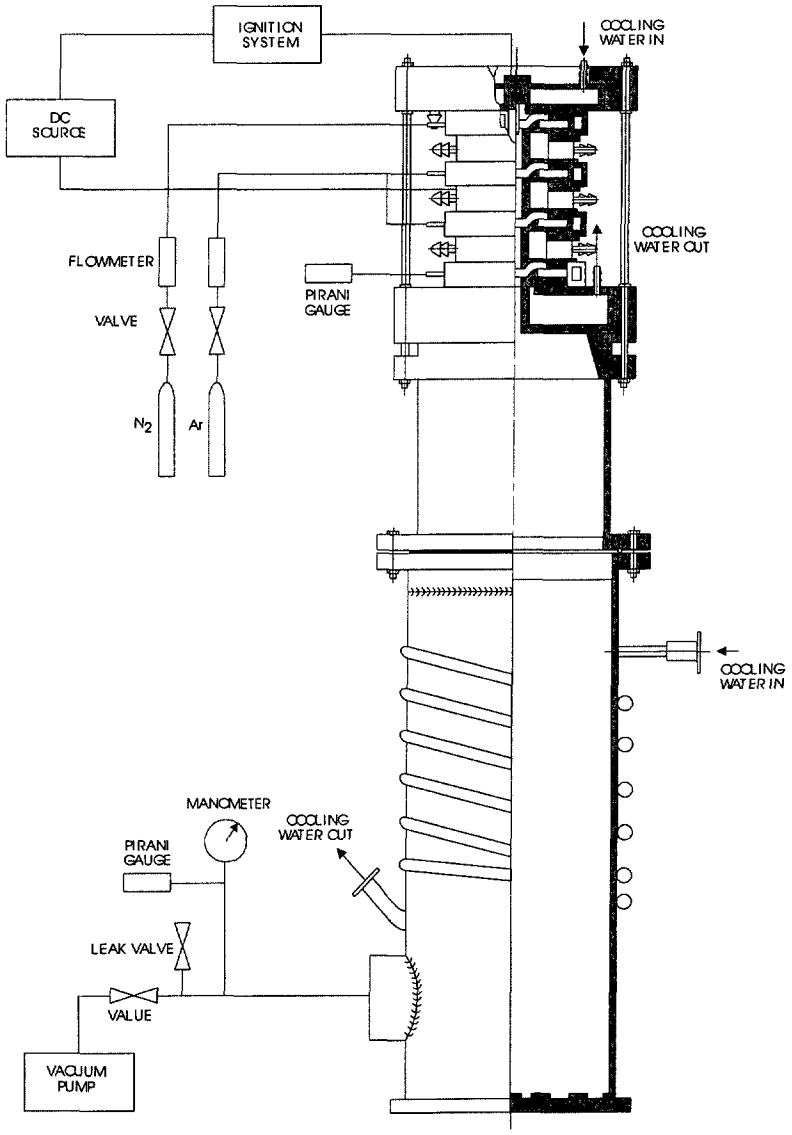

Fig. 1. — Experimental plasma source set-up.

laminar (Reynolds number is between 200 and 300). The different processes are stationary and thermodynamical equilibrium is obtained in the arc (thermal balance – one local temperature for all particles – and chemical equilibrium due to the pressure). With these assumptions, the temperature of arc and plasma jet can be calculated using energy equation for a single component gas. The stationary local energy equation (without axial thermal conduction) is:

$$\rho c_p v_z \frac{\partial T}{\partial z} + \rho c_p v_r \frac{\partial T}{\partial r} = \frac{1}{r}\frac{\partial}{\partial r}\left(\lambda r \frac{\partial T}{\partial r}\right) - u_r + \sigma E^2 \qquad (1)$$

where: T is the temperature, E is the electric field, ρ is the density of the gas, c_p is the specific heat at constant pressure, λ is the thermal conductivity, σ is the electric conductivity, v_z and v_r are the components of the velocity in the z direction (axis of the channel of the plasma torch) and in the r direction (radial axis), u_r is the radiation loss. In the arc and in the part of the plasma jet located in the core of the vortex, axial convection is preponderant compared to the radial convection because of thermal gradient and the axial velocity $V_z \gg V_r$. It can be neglected in equation (1). If we assume an uniform profile for ρv_z at the channel entrance of the plasma torch and parallel streamlines of flow in the core of the vortex, we obtain from the mass balance condition

$$\rho v_z = G/\pi r_c^2 \tag{2}$$

where: G is the mass flow rate, r_c is the radius of the channel of the plasma torch. This assumption presents the advantage to introduce the possibility of solving independently the energy balance of local mass balance equation. The axial electric field component E is given by

$$E = \frac{I}{2\pi \int_0^{r_c} \sigma r \mathrm{d}r}$$

where I is the arc current.

Introducing a heat flux potential defined by the relation $\mathrm{d}S = \lambda \mathrm{d}T$ and the velocity of the gas determined by (2), the temperature distribution in the arc and in the jet can be derived from the equation

$$\frac{G}{\pi r_c^2} \frac{c_p}{\lambda} \frac{\partial S}{\partial z} = \frac{1}{r} \frac{\partial}{\partial r} \left(r \frac{\partial S}{\partial r} \right) - u_r + \varepsilon \sigma E^2 \tag{3}$$

where $\varepsilon = 1$ for the arc and $\varepsilon = 0$ for the plasma jet in the channel in the region without electric field. The energy equation is solved using a regular and orthogonal grid in r and z coordinates. Following relationships are applied connecting the physical gas properties σ, u_r and the ratio c_p/λ to the heat flux potential for each step of the grid:

$$\sigma = a_{si,j} S, \qquad u_r = a_{ui,j} S, \qquad \frac{c_p}{\lambda} = a_{pi,j}. \tag{4}$$

The solution of stationary energy equation (3) for the arc and for the plasma jet needs the boundary conditions for the variable S and the partial derivative $\partial S/\partial r$. The four boundary conditions are specified:

- symmetry axis of the arc and the plasma jet: $\dfrac{\partial S}{\partial r}(0, z) = 0$,

- wall temperature condition: $S(r_c, z) = 0$ using a reference condition ($S = 0$) for the constant wall temperature,

- energy boundary condition at the cathode surface: $S(r, 0) = \varphi(r)$ with
  - $\varphi(r) = \dfrac{j^2}{4\sigma^2}(a^2 - r^2)$ for $0 < r < a$
  - $\varphi(r) = 0$ for $a \leq r \leq r_c$

where: j is the density of current on the cathode, a is the radius of the cathodic spot, σ_c is the electric conductivity of the gas closed the cathode, considering as constant value determined for $r = 0$,

- condition of continuity between the two zones in the channel (arc and jet)

$$S(r, z_{\text{jet}} = 0) = S(r, z_{\text{arc}} = l_{\text{arc}}) \qquad \text{for} \qquad 0 \leq r \leq r_{\text{c}}$$

where l_{arc} is the length of the arc. This length corresponds to the distance between the cathode surface and the first segment.

The cathode boundary condition assumes that the energy in the boundary layer is radially dissipated in the gas. Using 2×10^7 A m^{-2} as a constant current density j through the cathodic spot [12, 13] we determinate the radius a of the arc spot as a function of the arc current.

The solution of equation (3) can be represented as a series of Bessel functions multiplied by an exponential function:

$$S(r, z) = \sum_{n=1}^{\infty} R_n(r) Z_n(z) \tag{5}$$

where:

$$R_n(r) = A_n I_0(\mu r) + B_n Y_0(\mu r) \qquad Z_n(z) = C_n \exp\left(-\frac{\pi r_{\text{c}}^2}{G a_{p_i,j}} q_n^2 z\right)$$

and

$$\mu^2 = a_{\sigma_i,j} \varepsilon E^2 - a_{u_i,j} + q_n^2.$$

By application of the boundary conditions one obtains:

$$S(r, z) = \exp\left[\frac{\pi r_{\text{c}}^2}{G a_{p_i,j}} (a_{\sigma_i,j} \varepsilon E^2 - a_{u_i,j}) z\right] \sum_{n=1}^{\infty} A_n \delta \exp\left(-\frac{\pi \gamma_{\text{c}}^2}{G a_{p_i,j}} z\right) I_0\left(\frac{\gamma_n}{r_{\text{c}}} r\right) \tag{6}$$

where I_0 and Y_0 are Bessel functions of order zero of the first and second kinds, respectively, γ_n are roots of equation $I_0(\gamma_n) = 0$. The coefficients $A_n \delta$ are obtained from cathode boundary conditions for arc and condition of continuity between the two zones in the channel (arc and jet) for plasma jet; one finds that

$$A_n = \frac{2 j^2 r_{\text{c}}^3}{\gamma_n^3 I_1(\gamma_n) \sigma_{\text{c}} a}$$

and

$$\delta = 1 \qquad \text{for arc}$$

$$\delta = \exp\left[\frac{\pi r_{\text{c}}^2 l_{\text{arc}}}{G a_{p_i,j}} \left(a_{\sigma_i,j} E^2 - a_{u_i,j} - \frac{\gamma_n^2}{r_{\text{c}}^2}\right)\right] \qquad \text{for plasma jet}$$

The heat flux potential distribution of arc and plasma jet (6) are calculated simultaneously with a computation of the physical properties expressed as a function of the heat flux potential and the pressure. The thermal conductivity is calculated as a sum of three components: the thermal conductivity due to the particle translational energy, the thermal conductivity attached to the internal molecular energies and the thermal conductivity fraction which is due to the various chemical reactions (dissociation, ionization). The translational thermal conductivity is calculated using the second approximation of the Chapmann-Enskog method [14]. The reactive contribution is determined using the theory of Butler and Brokav [15] as extended to the case of partially ionized gases and internal thermal conductivity is calculated by Eucken method [16]. The different integrals of collisions have been determined by means of a potential of typical rigid spheres for neutral-neutrals interactions, dipole for ion-neutrals and electron-neutral interactions [14] and Debye for charged-charged interactions [17,18]. The gas density is

obtained using an ideal gas model. The specific heat coefficient at constant pressure is evaluated by a numerical differentiation of the total enthalpy which is the sum of the enthalpies of molecules, atoms, ions and electrons. The calculation of the specific heat coefficient at constant volume c_v, necessary for the calculation of the velocity of sound v_s [19] and to discriminate between the subsonic and supersonic regime of the flow, has been derived from a numerical differentiation of the internal energy determined from the enthalpy. The electric conductivity has been calculated from the expression [20] using the electron density, determined from the Saha law for equilibrium conditions. For argon, the radiation power in the energy equation has been calculated from the sum of the contributions of free – free radiation, line radiation and free – bound radiation [10]. For nitrogen, the emission coefficients deduced from the curves of reference [21].

3.2. Energy Transfer. — In order to evaluate the global energy distribution in the channel, the total electric input and radiation energy, the anode heat exchange and input and output convective energy are evaluated. These quantities are calculated by summing the values at each element of volume determined by indices i, j.

The arc plasma is created by Ohmic heating of the gas due to the current flowing between the cathode and the anode. Ohmic heat input is:

$$\begin{aligned} Q_{\text{Ohm}} &= \int\int\int_V \sigma E^2 \mathrm{d}V = 2\pi E^2 \int_0^{l_{\text{arc}}} \int_0^{r_c} \sigma(r,z) r \mathrm{d}r \mathrm{d}z \\ &= 2\pi E^2 \sum_i \sum_j a_{\sigma i,j} \sum_{n=1}^{\infty} A_n \delta \left\{ -\frac{Ga_{pi,j}}{\pi\gamma_n^2 + \pi r_c^2 (a_{ui,j} - a_{\sigma i,j}\varepsilon E^2)} \right. \\ &\quad \left. \times \exp\left[-\frac{\pi\gamma_n^2 + \pi r_c^2 (a_{ui,j} - a_{\sigma i,j}\varepsilon E^2)}{Ga_{pi,j}} z \right] \right\} \Bigg|_{l_{i-1}}^{l_i} \\ &\quad \times \frac{r_c}{\gamma_n} r I_1 \left(\frac{\gamma_n}{r_c} r \right) \Bigg|_{r_{j-1}}^{r_j} \end{aligned} \tag{7}$$

The absorption can be considered as negligible in the core of the plasma [22] and a strong absorption appears in the cold boundary layer along the wall. In this simple model the heat loss by radiation is calculated taken into account emission but not absorption. The total heat loss by radiation is then determined by the expression:

$$\begin{aligned} U_r &= \int\int\int_V u_r \mathrm{d}V = 2\pi \int_0^{l_{\text{arc}}} \int_0^{r_c} u_r(r,z) r \mathrm{d}r \mathrm{d}z \\ &= 2\pi \sum_i \sum_j a_{ui,j} \sum_{n=1}^{\infty} A_n \delta \left\{ -\frac{Ga_{pi,j}}{\pi\gamma_n^2 + \pi r_c^2 (a_{ui,j} - a_{\sigma i,j}\varepsilon E^2)} \right. \\ &\quad \left. \times \exp\left[-\frac{\pi\gamma_n^2 + \pi r_c^2 (a_{ui,j} - a_{\sigma i,j}\varepsilon E^2)}{Ga_{pi,j}} z \right] \right\} \Bigg|_{l_{i-1}}^{l_i} \\ &\quad \times \frac{r_c}{\gamma_n} r I_1 \left(\frac{\gamma_n}{r_c} r \right) \Bigg|_{r_{j-1}}^{r_j} . \end{aligned} \tag{8}$$

For calculation of conduction heat transfer, the anode is considered as thin walled ring. The exterior surface is water cooled, and the interior surface is heated by the arc. The heat flux on the surface is·

$$\mathbf{q}_{\text{cond}} = -\lambda \frac{\partial T}{\partial r} \mathbf{e}_r = -\frac{\partial S}{\partial r} \mathbf{e}_r \tag{9}$$

so the total conduction heat transfer in the anode is given by:

$$
\begin{aligned}
Q_{\text{cond}} &= -2\pi r_{\text{c}} \int_0^{l_{\text{arc}}} \frac{\partial S(r,z)}{\partial r} \mathrm{d}z \\
&= 2\pi \sum_i \sum_j \sum_{n=1}^{\infty} A_n \delta \left\{ -\frac{Ga_{pi,j}}{\pi\gamma_n^2 + \pi r_{\text{c}}^2 (a_{ui,j} - a_{\sigma i,j}\varepsilon E^2)} \right. \\
&\quad \left. \times \exp\left[-\frac{\pi\gamma_n^2 + \pi r_{\text{c}}^2 (a_{ui,j} - a_{\sigma i,j}\varepsilon E^2)}{Ga_{pi,j}} z \right] \right\} \Bigg|_{l_{i-1}}^{l_i} \\
&\quad \times \gamma_{\text{n}} I_1 \left(\frac{\gamma_n}{r_{\text{c}}} r \right) \Bigg|_{r_{j-1}}^{r_j} .
\end{aligned} \tag{10}
$$

The convective heat flux passing through the surface for $z = 0$ and $z = l_{\text{arc}}$ takes the form:

$$
\begin{aligned}
Q_{\text{conf}} &= \int_s \rho v_z c_{\text{p}} T \mathrm{d}s = \frac{2G}{r_{\text{c}}^2} \int_0^{r_{\text{c}}} \frac{c_{\text{p}}(r,z)}{\lambda(r,z)} S(r,z) r \mathrm{d}r \\
&= \frac{2G}{r_{\text{c}}} \sum_i \sum_j \sum_{n=1}^{\infty} A_n \delta a_{pi,j} \exp\left[-\frac{\pi\gamma_n^2 + \pi r_{\text{c}}^2 (a_{ui,j} - a_{\sigma i,j}\varepsilon E^2)}{Ga_{pi,j}} z \right] \Bigg|_{i-1}^{l_i} \frac{r}{\gamma_n} I_1 \left(\frac{\gamma_n}{r_{\text{c}}} r \right) \Bigg|_{r_{j-1}}^{r_j}
\end{aligned} \tag{11}
$$

In the balance energy equations the difference between heat flux passing through the surface for $z = 0$ and heat flux through the surface $z = l_{\text{arc}}$ is taken into account.

3.3. METHOD OF CALCULATION. — The heat flux potential distribution (6) is determined with three subroutines and a main program. The POTENTIAL subroutine calculates the coefficient λ and the heat flux potential S as a function of the temperature and the pressure. The subroutine PROPERTY calculates parameters c_{p}, c_{v}, ρ, v_s and σ as a function of temperature and the pressure. The internal energy is also calculated by this subroutine. The COEFFICIENT subroutine gives an approximation for coefficients a_p, a_u and a_σ by a constant value or by a linear approximation in each interval ΔS of the heat flux potential.
The main program PAPYRUS has three functions:
1) determination of the boundary conditions for the jet from the energy equation of the arc,
2) calculation of the field $S(z, r)$ and the velocity field in the plasma jet and the field of temperature,
3) calculation of energy transfer using the fields of heat flux potential in the arc and in the plasma jet.

In the calculation of fields, the arc is divided following its length in n equal parts and following the radius in p equal parts, forming thus $n \times p$ identical elements of volume. First, the heat flux potential distribution is determined in the section of the arc for $z = 0$. By using this distribution of $\varphi(r)$, coefficients a_p, a_r and a_σ had been chosen for $j = 1$ and $i = 1, \ldots p$. The heat flux potential is then calculated, coefficients being modified at each step of the grid.

Calculated profiles at the extremities of the arc are used to initialize the calculation in the plasma jet. Using the same grid following the variable r the heat flux potential distribution in the plasma jet is obtained. Next the energy transfer is calculated applying the fields of heat flux potential in the arc and in the plasma jet.

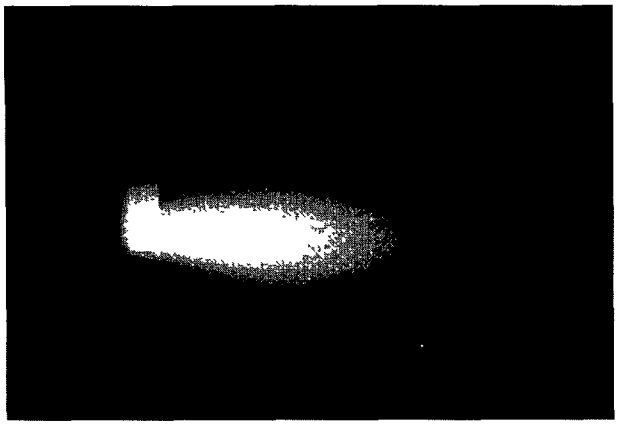

Fig. 2 — Ellipsoidal subsonic plasma jet, argon, 26.6 kPa, 70 A, 0.4 g s^{-1}

4. Regimes of Flow

Experiments have been performed with argon and nitrogen for different mass flow rates, between 0.04 g s^{-1} and 1.2 g s^{-1}, and for a static pressure measured in the chamber of the plasma torch in the range of 10–100 kPa. The arc currents have been in the range of 80–300 A. The velocity, temperature and energy transfer have been calculated and discussed for the experimental conditions.

It should be noted that the calculated temperature is function of the current density on the cathode surface. A change in current density by a factor 2 induces a change in temperature at the cathodic region by about 35%. However, the difference of temperature at the torch exit is less important and is estimated to be 15%. The results show that the variation of 20% on the value of the electric field induces only a variation of 5% on the temperature in the developed arc region. Because of that, the calculated distributions depend on arc current and arc voltage determined by experiments.

4.1. Subsonic Plasma Flow. — At a higher mass flow rate then 0.1 g s^{-1} the flow remains subsonic for the used range of arc current. The shape of the plasma jet is similar to the jet showed in Figure 2 for an arc current lower than 90 A, or with an identical shape as presented in Figure 3 for an arc current higher than 90 A. For low arc current, the jet has quasi-ellipsoidal contours. For high arc currents, a luminous core appears and the shape of the subsonic plasma jet is then always conical until its interaction with the wall chamber in quartz. The increase of the arc current for the following range of mass flow rate, 0.1 g s^{-1} – 0.5 g s^{-1}, induces an increase of the diameter of the luminous core while its length remains quasi constant. For a mass flow rate up to 0.8 g s^{-1}, not only the diameter of the luminous core increases considerably with the increase of the arc current but also its length. For experimental conditions for pressure, mass flow rate and arc current, there is no shock wave in the plasma jet confirming the subsonic velocity of the flow. The argon arc voltage is decreasing from 42 V to 28 V and the electric power is quasi linear rising from 3 kW to 8.2 kW for the argon arc.

The calculated temperature and velocity distributions in jet at the plasma torch exit is presented in Figure 4 for a pressure in the chamber of 26.6 kPa and for a mass flow rate of 0 5 g s^{-1}. The temperature is increasing from 6220 K to 12 500 K on the plasma jet axis ($r = 0$), for an arc current varying from 80 A to 280 A. It should be noted that the increase of

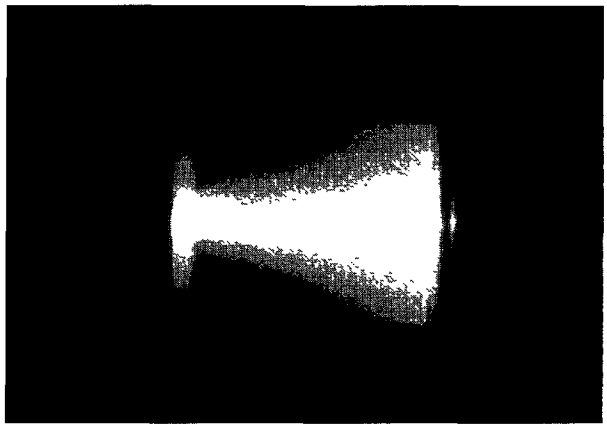

Fig. 3 — Conical subsonic plasma jet, argon, 26 6 kPa, 190 A, 0.4 g s^{-1}.

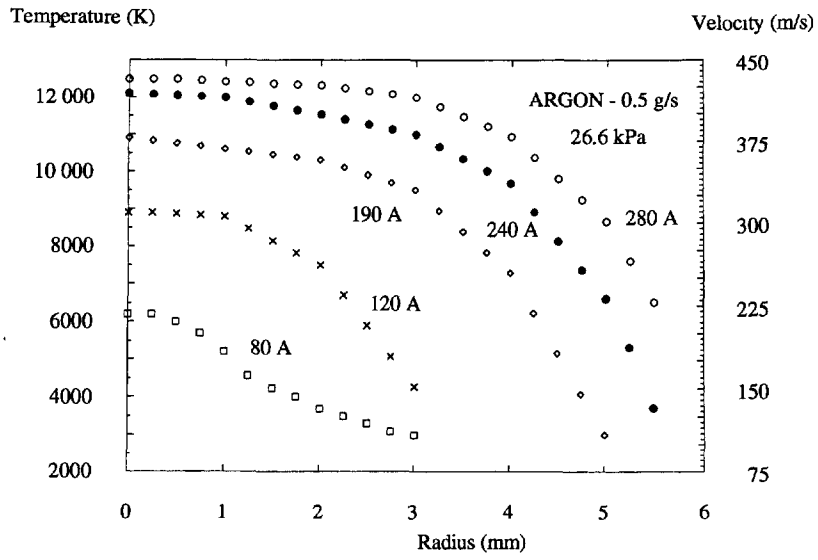

Fig 4. — Temperature and velocity distributions at the plasma torch exit

the arc current induces the appearance of a uniform zone in temperature greater, in the order 6 mm of diameter for an arc current of 280 A. The velocity on the plasma jet axis is increasing with the arc current from 210 m s^{-1} to 430 m s^{-1} and the Mach number increase from 0.15 to 0.27 (Fig. 5). The increase of the mass flow rate induces an important increase of the velocity from 430 m s^{-1} to 930 m s^{-1} for an arc current of 280 A and the Mach number reaches 0.6 (Fig. 5). This effect is explained by relation (2) where the velocity is proportional to the mass flow rate but also by the variation of the mass density due to the variation of the temperature; the increase of the mass flow rate entailing a growth of the temperature. This influence of the mass flow rate to temperature is explained by the variation of the power transmitted to the arc.

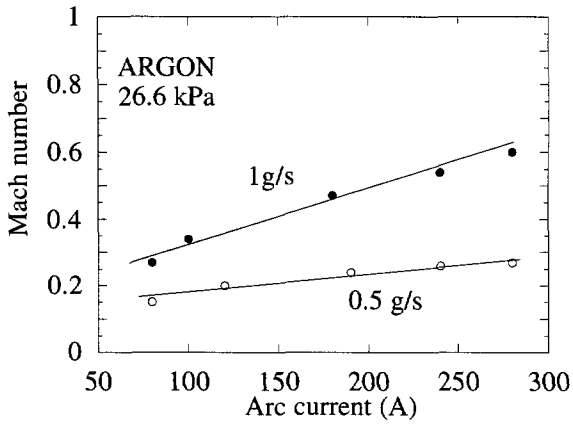

Fig 5. — Mach number as a function of arc current.

The calculations of energy transfer show that radiation loss is most important for the arc current of 200 and 250 A. For these values of arc current the radiation loss is respectively 82% and 86% of the Ohmic heating. The conduction heat transfer in the anode is below 15%. The radiation loss decreases with arc current and for the value of 160 A we estimate as 20.6%. The convective heat flux passing through the surface for $z = l_{arc}$ increases from 736 W for arc current of 160 A to 1166 W for current of 250 A.

Plasma jet exiting the channel of the plasma torch is characterized by a luminous core. With assumption that this core corresponds to a temperature up to 6000 K, it is possible to compare the diameter of the calculated core and the diameter deduced by photography. The limit to 6000 K is chosen by reason of the sharp decrease in the electric conductivity to this temperature. Figure 6 shows the good agreement between calculated results and measured results. It can be seen that the diameter increases with the arc current and that mass flow rate has no significant influence on this diameter.

Nitrogen plasma jets have a similar shape as argon jets but for an arc current up to 120 A, they present a core more luminous than for argon and have a length equal to that of the quartz cylinder. For nitrogen, the arc voltage is decreasing from 65 to 30 V and the electric power is quasi linearly increasing from 5.9 to 11.2 kW.

For a pressure in the chamber of 26.6 kPa and for a nitrogen mass flow rate of 0.5 g s^{-1}, the calculated temperature (Fig. 7) is increasing from 7200 K to 12 000 K at the plasma torch exit and on the jet axis ($r = 0$) for an arc current varying from 120 A to 280 A. The argon plasma temperature is higher than the nitrogen with a difference of 1000 K although the electric power is lower. The nitrogen plasma velocity on the jet axis is varying from 350 to 610 m s^{-1} (Fig. 7) while being superior to that of argon, at an arc current of 280 A, it is 610 m s^{-1} in nitrogen and 430 m s^{-1} in argon. Mach numbers vary from 0.24 for a mass flow rate of 0.5 g s^{-1} to 0.68 for a mass flow rate of 1.1 g s^{-1} (Fig. 8) A calculation of the radius of the plasma jet for the two values of mass flow rate: 0.5 and 1.1 g s^{-1}, shows a good agreement with experimental measurements (Fig. 9).

4.2. Supersonic Plasma Flow. — For a pressure in the chamber of 10.6 kPa, a mass flow rate of 0.04 g s^{-1} and for arc current up to 180 A, a cylindrical plasma jet has been observed with a diameter corresponding to the diameter of the plasma torch exit (Fig. 10). The luminous part of the jet is approximately 1 m long. In an intermediate configuration for the jet, a first

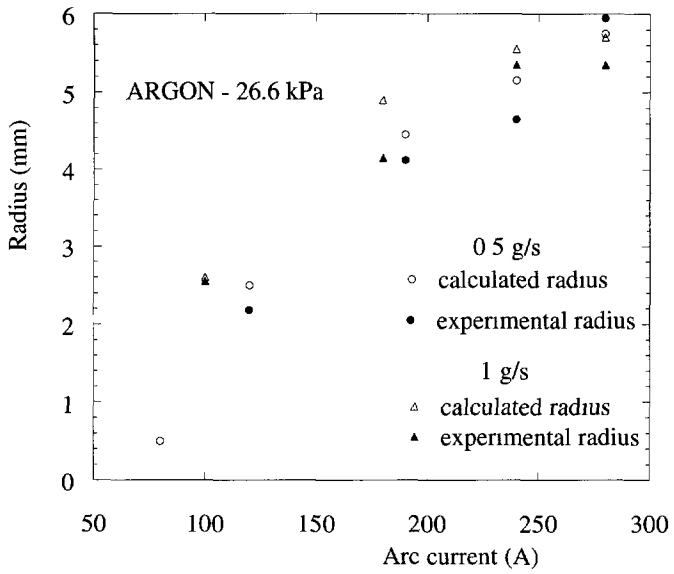

Fig. 6. — Calculated and experimental radius as a function of arc current.

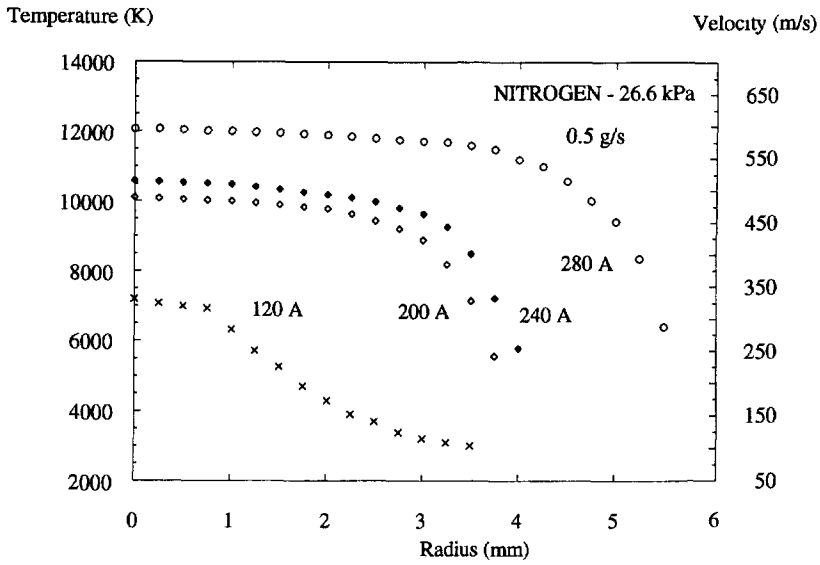

Fig 7. — Temperature and velocity distributions at the plasma torch exit.

cylindrical part at the plasma torch exit then a conical part (Fig. 11) are observed. It should be noted that cylindrical jets are more easily obtained with argon compared to nitrogen. For example, with a longer nitrogen arc (between the cathode and the second segment), a cylindrical plasma jet is not obtained while argon jets take this form for more high currents. The passage to the cylindrical form of the jet is often associated to an erosion of the cathode, this erosion is not observed in the case of the stable cylindrical jet.

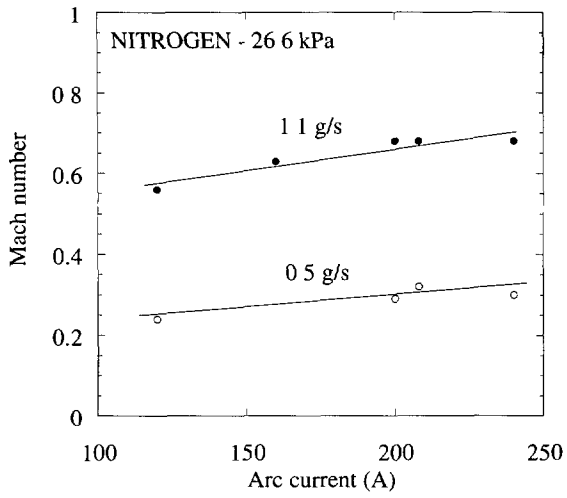

Fig. 8. — Mach number as a function of arc current

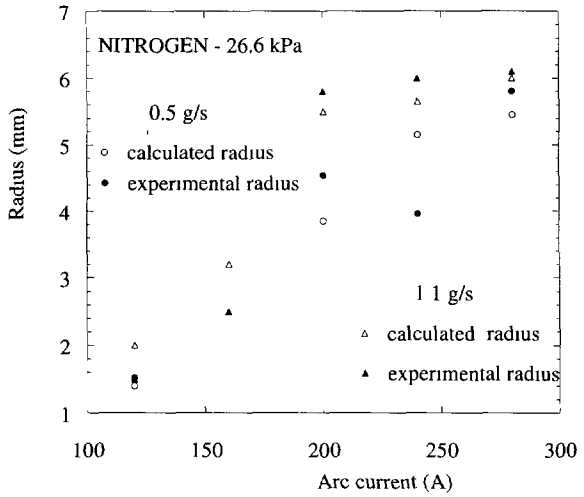

Fig. 9. — Calculated and experimental radius as a function of arc current.

Calculations for experimental conditions in which cylindrical jets are obtained, have shown that for the cylindrical jet at the plasma torch exit in a first part and then conical in a second part, the velocity is approximately equal to the sound velocity. Cylindrical jets correspond to light supersonic flows since the calculated Mach numbers are between 1.04 and 1.08, velocities at the plasma torch exit are between 1750 m s^{-1} and 2150 m s^{-1} and temperatures are between 9800 K and 13 800 K for nitrogen (Fig. 12). One should note that the temperature for supersonic cylindrical jets is superior to the temperature of subsonic jets. Both experiments and calculations shown that the region with a strong thermal gradient that is situated between the high temperature core and the surrounding cold region is very thin.

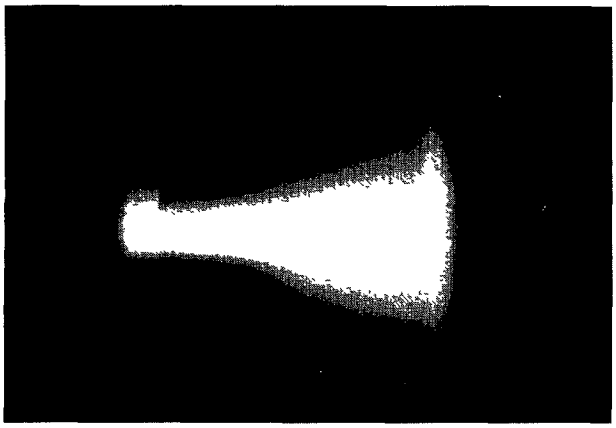

Fig. 10 — Supersonic plasma jet, $M \approx 1$, argon, 10.6 kPa, 180 A, 0.08 g s^{-1}.

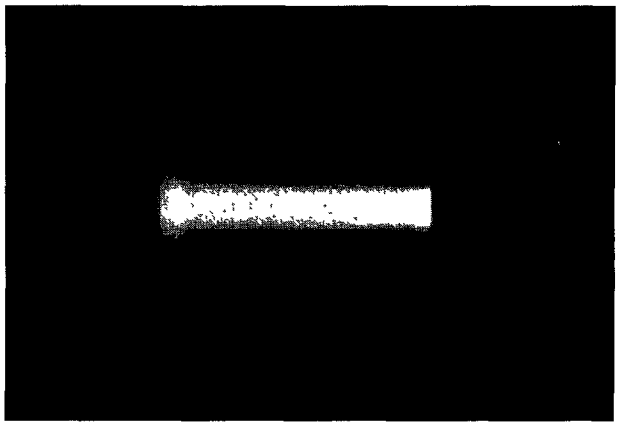

Fig 11 — Supersonic plasma jet, $M > 1$, argon, 10.6 kPa, 280 A, 0.04 g s^{-1}.

The calculations of energy transfer show that in supersonic regime, the radiative terms are small compared to subsonic regime. In the argon arc, the calculated radiation loss presents 44% of the Ohmic heating for arc current of 280 A and only 7% for arc current of 180 A. The convective heat flux through the surface for $z = l_{arc}$ is 3881 W for arc current of 280 A and 1156 W for current of 180 A.

5. Conclusions

The subsonic plasma jets with the diffusive forms and supersonic cylindrical jets in argon and nitrogen in low pressure chamber using the plasma torch with segmented anode were obtained. The different regimes of plasma flow are obtained for specified conditions of plasma torch operating parameters and pressure in chamber. Based on the LTE assumption, simple and successful calculation have been performed for predicting the conditions of generating supersonic and subsonic plasma jets using only energy equation. These calculations allow to analyse the temperature, velocity and shape of plasma jets for operating parameters of plasma

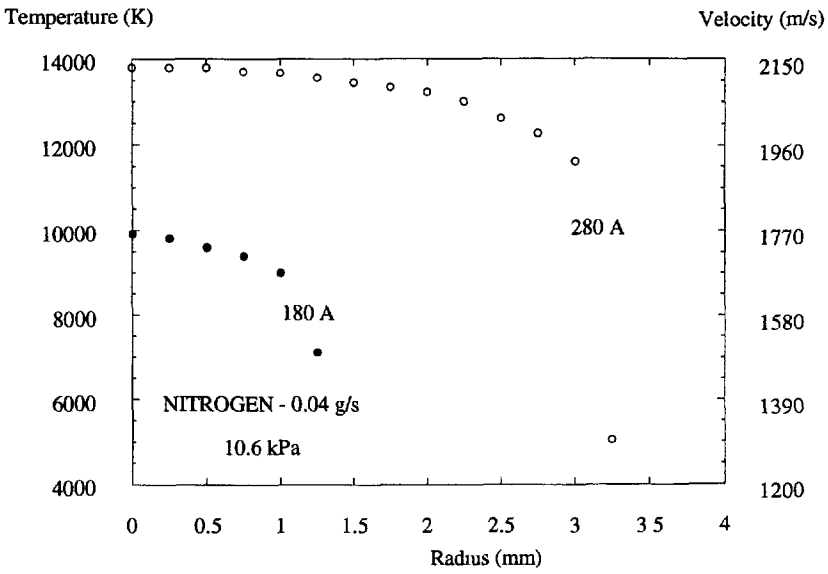

Fig. 12. — Temperature and velocity distributions for a cylindrical jet at the plasma torch exit.

torch such as arc current, gas flow rate and pressure in the chamber. The energy transfer for subsonic and supersonic jets is also calculated and discussed.

The results show that cylindrical jets correspond to light supersonic flows with the Mach numbers between 1.04 and 1.08. The subsonic jets have diffusive shape and the Mach number is below 0.6. The temperature for supersonic cylindrical jets is greater than the temperature of subsonic jets. The calculations of energy transfer show that in supersonic regime, the radiative term is small and axial convective heat flux is large compared to subsonic regime.

We have shown the possibility of a simple analyse of a plasmatron by the energy equation. However, a necessary precise validation is planed to confirm the temperature profiles by optical emission spectroscopy.

References

[1] Griem H R., Plasma Spectroscopy (Mc Graw-Hill Book Company. New York, 1964).
[2] Drawin H.W., Validity Conditions for Local Thermodynamic Equilibrium, Progress in Plasmas and Gas Electronics, Vol. 1 (Akademie-Verlag, Berlin, 1974).
[3] Kafrouni H., Bagneux J.M., Gleizes A. and Vacquié S , Temporal changes of particle densities and temperatures in decaying arc discharge, *J. Quant. Spectrosc. Radiat. Transfer* **21** (1979) 185-201.
[4] Baitin A.V., Fedotov V.Yu., Ivanov A.A., Karetnikov M.D and Serov A.A , Stationary Discharges for Plasma Chemistry, IAE 5899/7 (1995) 1-42.
[5] Haidar J.. Local thermodynamic equilibrium in the cathode region of a free burning arc in argon, *J. Phys. D: Appl. Phys.* **28** (1985) 2494-2504.

[6] Meulenbrocks R.F.G., Engeln R.A.H., Beurskens M.N.A., Paffen R.M.J., van de Sanden M.C.M., van der Mullen J.A.M. and Schram D.C., The argon-hydrogen expanding plasma: model and experiments, *Plasma Sources Sci. Technol.* **4** (1995) 74-85.

[7] Megli T.W., Krier H. and Burton R.L., A Plasmadynamics Model for Nonequilibrium processes in N_2/H_2 Arcjets, AIAA Paper 95-1961, 26th AIAA Plasmadynamics and Lasers Conf., June 19-22 (San Diego,CA, 1995).

[8] Sleziona P.C., Auweter-Kurtz M. and Messerschmid E.W., Numerical Model for a Plasma Wind Tunnel Accelerator, AIAA Paper 95-2110, 30th AIAA Thermophysics Conf., June 19-22 (San Diego, CA, 1995).

[9] van de Sanden R., The expanding plasma jet: experiments and model, Ph. D. Thesis (University of Technology, Eindhoven, The Netherlands, 1991).

[10] Beulens J.J., Milojevic D., Schram D.C. and Vallinga P.M., A two-dimensional nonequilibrium model of cascaded arc plasma flows, *Phys. Fluids B* **3** (1991) 2548-2557.

[11] Chang C.H. and Pfender E., Nonequilibrium modeling of low-pressure argon plasma jets, *Plasma Chem. Plasma Processing* **10** (1990) 493-491.

[12] Hsu K. and C. Pfender E , Analysis of the cathode region of a free-burning high intensity argon arc, *J. Appl. Phys.* **54** (1983) 3818-3824.

[13] Delalondre C., Modélisation aérodynamique d'arcs électriques à fortes intensités avec prise en compte du déséquilibre thermodynamique local et du transfert thermique à la cathode, Ph. D. Thesis (Rouen University, France, 1990).

[14] Hirschfelder J.O., Curtis C. F. and Bird R.B., Molecular theory of gases and liquids (John Wiley & Sons, 1970)

[15] Butler J.N. and Brokaw R S., Thermal conductivity of gas mixtures in chemical equilibrium, *J. Chem. Phys.* **26** (1957) 1636-1643.

[16] Aubreton J. et Fauchais P., Influence des potentiels d'interaction sur les propriétés de transport des plasmas thermiques : exemple d'application le plasma argon - hydrogène à la pression atmosphérique, *Rev. Phys. Appl.* **18** (1983) 51-66.

[17] Devoto R.S., Simplified expressions for the transport properties, *Phys. Fluids* **10** (1967) 354-364.

[18] Bonnefoi C., Contribution à l'étude des méthodes de résolution de l'équation de Boltzmann dans un plasma à deux températures : exemple le mélange argon-hydrogène, Ph. D. Thesis (Limoges University, France, 1983).

[19] Kaminska A., Models of electric arc, Rap. KBN nr PB 031/P4/93 (Poland, 1993).

[20] Mitchner M. and Kruger C.H., Partially Ionized Gases (Wiley & Sons, New York, 1973).

[21] Gleize A., Rahamani B., Gonzales J.J. and Liami B., Calculation of net emission coefficient in N_2, SF_6 and $SF_6 - N_2$ arc plasmas, *J. Phys. D: Appl. Phys.* **24** (1991) 1300-1309.

[22] Zukov M.F. and Korotjejev A.S., Theory of Arc Plasma (Nauka Ed., Novosybirsk, 1987).